

Article

Study of the Adsorption of Anionic Surfactants on Carbonate Rocks: Characterizations, Experimental Design, and Parameter Implementation

Valdivino Francisco dos Santos Borges ^{1,2,*} , Mayra Kerolly Sales Monteiro ³ , Ernani Dias da Silva Filho ⁴ , Dennys Correia da Silva ⁴, José Luís Cardozo Fonseca ¹, Alcides O. Wanderley Neto ¹ and Tiago Pinheiro Braga ¹ 

¹ Institute of Chemistry, Postgraduate Program in Chemical—PPGQ, Federal University of Rio Grande do Norte, New Lagoon District, Natal 59078-970, RN, Brazil; jose.fonseca@ufrn.br (J.L.C.F.); alcideswanderley@hotmail.com (A.O.W.N.); tiagoquimicaufm@gmail.com (T.P.B.)

² Institute of Education, Science and Technology of Rondônia (IFRO), Amazon River Street, 151-Migrant Garden, Ji-Paraná 76900-730, RO, Brazil

³ Laboratory of Environmental and Applied Electrochemistry—LEAA, Postgraduate Program in Chemical Engineering—PPGEQ, UFRN, New Lagoon District, Natal 59078-970, RN, Brazil; mayra.kerolly@gmail.com

⁴ Department of Petroleum Engineering, Federal University of Rio Grande do Norte, New Lagoon District, Natal 59064-970, RN, Brazil; ernanidasilv@gmail.com (E.D.d.S.F.); dennys.silva19@gmail.com (D.C.d.S.)

* Correspondence: valdivinofrancisco211@gmail.com or valdivino.santos@ifro.edu.br (V.F.d.S.B.); Tel.: +55-84-996078949

Abstract: Controlling or reducing the adsorption of surfactants on reservoir rock surfaces has been a challenging task in enhanced oil recovery (EOR) methods, as it directly affects the cost-effectiveness of the projects. The adsorption of surfactants on rock surfaces can modify their hydrophobicity, surface charge, and other important parameters that govern EOR processes, such as reducing the interfacial tension between water and oil and increasing permeability. Therefore, understanding the adsorption mechanism on rocks is essential for developing alternatives that improve the effectiveness of these processes. In this work, the adsorption of surfactants on carbonate materials was evaluated considering variations in temperature, contact time, and surfactant concentration. The surfactants used were derived from vegetable oils, aiming for a sustainable approach: saponified coconut oil (SCO), saponified babassu coconut oil (SBCO), and saponified castor oil (SMO). The finite bath method was used, resulting in adsorption efficiencies of 85.74%, 82.52%, and 45.30% for SCO, SBCO, and SMO, respectively. The Sips isotherm and the pseudo-second-order model were found to be suitable for characterizing these systems. The simulation of SCO adsorption isotherms on limestone by the Langmuir model was more accurate than that using the Freundlich model. The limestone showed a negative surface charge of approximately -35.0 mV at pH 6.5; this negative charge varied over a wide pH range. These zeta potential data for the samples confirmed that hydrophobic interactions played an important role in the adsorption of the surfactants. Thermodynamic evaluation indicated spontaneous and endothermic adsorption of SCO on limestone. The systems were also characterized by FTIR, TG/DTG, XRD, XRF, SEM, and zeta potential.

Keywords: adsorption; anionic surfactants; carbonate materials; adsorption efficiency; isotherms



Citation: Borges, V.F.d.S.; Monteiro, M.K.S.; Filho, E.D.d.S.; Silva, D.C.d.; Fonseca, J.L.C.; Neto, A.O.W.; Braga, T.P. Study of the Adsorption of Anionic Surfactants on Carbonate Rocks: Characterizations, Experimental Design, and Parameter Implementation. *Coatings* **2024**, *14*, 856. <https://doi.org/10.3390/coatings14070856>

Received: 10 May 2024

Revised: 26 June 2024

Accepted: 30 June 2024

Published: 8 July 2024



Copyright: © 2024 by the authors. Licensee MDPI, Basel, Switzerland. This article is an open access article distributed under the terms and conditions of the Creative Commons Attribution (CC BY) license (<https://creativecommons.org/licenses/by/4.0/>).

1. Introduction

The pursuit of sustainable solutions in the oil and gas industry has led to the exploration of biodegradable alternatives for enhanced hydrocarbon recovery. Factors such as wettability and high interfacial tensions can affect the oil recovery process, and one of the methods for maximizing oil production is the injection of surfactants. Surfactant adsorption is a very complex phenomenon that significantly influences the economics of the surfactant injection process. The use of surfactants in reservoirs aims to reduce interfacial tensions, increasing flow and oil recovery. In this context, the study of adsorption of

biodegradable anionic surfactants on carbonate rocks emerges as a rapidly growing area of interest [1–6]. Carbonate rocks, including limestone and dolomite, are significant components of petroleum reservoirs [7–12]. Their unique surface and mineralogical properties directly influence the adsorption of surfactants, playing a crucial role in the effectiveness of recovery processes [13–16] and requiring precise characterization of carbonate rocks, combined with detailed analysis of surfactant–rock interactions [17–26].

Surfactant adsorption has been studied for decades, with parameters such as molecular structure, temperature, electrolyte concentration, ionic strength, and pH being extensively investigated. Soumik Das et al. [17] explored the adsorption of non-ionic surfactants on carbonate surfaces and found that secondary alcohol ethoxylate and nonylphenol ethoxylate effectively alter the wettability of these surfaces. This phenomenon, attributed to the amphiphilic nature of surfactants, enhances oil displacement efficiency and sweep capacity [27]. In this context, Kun Ma et al. [28] studied the adsorption of cationic and anionic surfactants on carbonate materials. They observed that cetylpyridinium chloride had insignificant adsorption, while sodium dodecyl sulfate (SDS) precipitated in the presence of CO₂. Such findings highlight the influence of the carbonate and/or sandstone source on the adsorption of ionic and non-ionic surfactants, which may affect oil recovery [29,30].

A prime factor for the effectiveness of surfactants in altering reservoir wettability is the amount adsorbed on mineral surfaces [31]. Indeed, it is crucial to understand the surfactant–substrate interactions governing adsorption and to obtain representative adsorption isotherms [27,28,30,32–34]. Several authors have studied how surfactant adsorption affects wettability and oil recovery in different types of rocks [34–40]. Among biodegradable surfactants, saponified coconut oil, saponified castor oil, and other natural derivatives have received attention. These compounds, resulting from the saponification process, possess hydrophobic chains that interact with the surface of carbonate rocks [32]. Saponified coconut oil, for example, is rich in fatty acids and natural surfactants, which have shown promising properties in reducing interfacial tensions between oil and water, a crucial factor in hydrocarbon recovery [3,29,41,42].

This article presents a comprehensive study of the adsorption of biodegradable anionic surfactants on carbonate rocks. The aim was to treat the surface of reservoir rocks with biodegradable surfactants as sustainable alternatives for advanced oil recovery. The investigation was conducted through a multidisciplinary approach, which encompassed meticulous characterizations of the rocks, careful experimental design, and systematic analysis of relevant parameters. By establishing correlations between experimental results and theoretical models, it was possible to elucidate the main determinants of adsorption, thus contributing to informed decision-making in the development of sustainable oil recovery processes. This approach employs an innovative method with the use of biodegradable surfactants for the treatment of reservoir rocks and thus has the potential to become a valuable method since there is no advanced work related to these surfactants for this purpose.

2. Materials and Methods

2.1. Materials

The adsorbents used in this study were carbonate rocks. The rock samples were collected from the Botucatu formation in the state of Rio Grande do Norte, Brazil, and were ground in a ball mill for 24 h. Subsequently, a calcination process was carried out to remove moisture and organic materials present in the rock pores, aiming to increase their permeability. The samples were placed in a muffle furnace for a period of 6 h at a temperature of 250 °C, with a heating rate of 10 °C per minute, under air atmosphere [10–12,32].

Subsequently, the samples were sieved with mechanical agitation through a series of sieves, ranging from 48 to 100 mesh, aiming to obtain a granular solid in homogeneous fractions. This process lasted approximately 10 min, and the fractions corresponding to 100 mesh were collected.

The biodegradable surfactants were synthesized in the laboratory through a saponification reaction. To obtain the surfactants, 100 g of vegetable oil (coconut, babassu coconut,

or castor oil), 300 mL of ethyl alcohol, and a solution of sodium hydroxide (Synth, 100%) were added to a 1000 mL round-bottom flask. This flask was attached to a reflux condenser and heated on a heating mantle until the reaction was completed, as suggested by Silva et al. [43]. Abbreviations of the surfactants used: saponified coconut oil (SCO), saponified babassu coconut oil (SBCO), and saponified castor oil (SMO). All solutions were prepared with deionized water.

2.2. Methods

2.2.1. Correlation between Surfactant Concentration and Surface Tension

It is known that different concentrations of surfactants, when they are below the Critical Micelle Concentration (CMC), may be linearly correlated with surface tension values [35]. Measuring the surface tension of a surfactant solution under the mentioned conditions allows the determination of the surfactant concentration value present in that medium through linear regression adjustment [23,24,44,45].

Given this fact, concentration curves of surfactant versus surface tension were constructed to determine the linear equations correlating surfactant concentrations with surface tensions and, consequently, to determine the Critical Micelle Concentration (CMC) of each surfactant, which corresponds to the point of intersection between the linear curve and the constant curve on the graph. For the construction of the mentioned graphs, initial solutions of each of the surfactants were prepared at a concentration of 5% (*w/w*). The QC6000 equipment from SensaDyne Instruments was used, employing the maximum bubble pressure method to measure surface tension.

Sequential dilutions were performed until the results approached 72 Dynes/cm, which corresponds to the surface tension of water. The temperature used for the tests was 27 ± 1 °C, as previous studies have shown that an increase in temperature does not cause significant differences in CMC values [35].

2.2.2. Finite Bath Adsorption Tests

In brief, 1 g of carbonate rock was placed in a 250 mL Erlenmeyer flask. Next, a predetermined amount of surfactant solution at a concentration of 0.3% above the CMC of each surfactant was added. The aim of this concentration increase was to reduce the likelihood of interface saturation [23]. The samples were then placed in a thermostatic bath (Dubnoff water bath, model TE-053, Tecnal manufacturer, São Paulo, Brazil) and stirred constantly at 50 rpm. After reaching the desired contact time, filtration (14 µm, Ø = 11 cm) was performed to separate the rock grains from the surfactant solution.

The surface tensions of the filtrates were measured to determine any increase in tension, indicating a change in surfactant concentration (final concentration, C_e).

The surfactant adsorption efficiency (AE) onto the inert rock is calculated by Equation (1).

$$AE = \frac{C_o - C_e}{C_o} \cdot 100 \quad (1)$$

where C_o (mg/mL) is the initial concentration of surfactant (before adsorption) and C_e (mg/mL) is the equilibrium concentration or final concentration after the solution has been in contact with the rock.

2.2.3. Experimental Design—Evaluation of Systems with Higher Adsorption Capacity

The analysis of surfactant adsorption on rocks was carried out through a factorial experimental design of type 2^3 with three replications at the central point. Each batch consisted of 11 tests of surfactant solution assays with concentrations exceeding the CMC (0.3%). The selected study variables included the rock quantity to surfactant solution volume ratio (R/S), the contact time between the surfactant solution and the rock (h), and the test temperature (°C). The response variable was the surfactant adsorption efficiency (AE%) on the rock. All tests were performed in duplicate. The levels of each factor are presented in the Supplementary Materials in Table S1

After the statistical experimental design, the adsorption test with the highest capacity for each surfactant (referred to as the optimal point) was subsequently chosen to study the evaluation of adsorption kinetics and the properties of limestone before and after adsorption. This optimal point parameter was chosen so that the highest amount of surfactant adsorption would maximize the differences in the rock before and after the adsorption tests.

2.2.4. Rock Characterization

X-Ray Fluorescence (XRF)

The chemical composition of the adsorbents (limestone rock) was analyzed using X-ray fluorescence with the Bruker S2 Ranger equipment, employing Pd or Ag anodes with a maximum power of 50 W, 50 kV, 2 mA current, and a Silicon X Flash detector, at a temperature of 298 K.

X-Ray Diffraction

For mineralogical characterization, the Bruker D2 Phaser diffractometer was used with copper radiation ($\text{CuK}\alpha$, $\lambda = 1.54 \text{ \AA}$) and a Ni filter. A voltage of 30 kV, 10 mA current, and Lynxeye detector were used. The data collected were analyzed across a broad range of Bragg angle 2θ degrees, spanning from 10° to 80° , with a step size of 0.02° , an acquisition time of 0.1 s, and at a temperature of 298 K.

Differential Thermal Analysis and Thermogravimetric Analysis (DTA/TGA)

Thermogravimetric analysis (TGA/DTG) of the adsorbent materials was performed using the thermal analysis system, model SDTQ600 from TA Instruments. The atmosphere used was nitrogen ($100 \text{ mL}\cdot\text{min}^{-1}$), with a heating rate of $10 \text{ }^\circ\text{C}\cdot\text{min}^{-1}$, in the temperature range from ambient to $1000 \text{ }^\circ\text{C}$. Platinum crucibles and approximately 10 mg of samples were used for all analyses.

Fourier Transform Infrared Spectroscopy (FTIR)

Fourier transform infrared spectroscopy (FTIR) analyses were performed using the IRAffinity-1 apparatus from Shimadzu, coupled with an HATR MIRacle module with a ZnSe prism. A mid-infrared beam with a wavelength range of 2.5 to $50 \text{ }\mu\text{m}$ was utilized, covering a wavenumber range of 4000 to 500 cm^{-1} .

Zeta Potential

To analyze the electric charges of limestone particles, the zeta potential analyzer, ZetaPlus, from Brookhaven Instruments Corporation, was utilized. To evaluate the behavior of the zeta potential as a function of pH, as suggested in previous studies [39,40], solutions were adjusted to pH values of approximately 2, 4, 6, 8, 10, and 12. Hydrochloric acid 0.01 M solution (HCl—37%, Synth) and sodium hydroxide 0.01 M solution (NaOH—100%, Synth) were employed to adjust the pH. Each measurement was repeated ten times, and the final average was calculated.

Scanning Electron Microscopy (SEM)

Scanning electron microscopy analyses of the samples were performed using a Hitachi tabletop microscope, model TM-3000, with an acceleration voltage between 5 and 15 kV and magnifications ranging from 500 to 4000 times.

2.2.5. Static Adsorption Test

To evaluate the effectiveness of adsorption on the adsorbent solids, the final solute concentration (C_e) and the amount of surfactant adsorbed on the adsorbent surface were determined through a mass balance, using the calculation of adsorption capacity (Equation (2)).

$$q = \frac{(C_0 - C_e)V}{m} \quad (2)$$

where q is the adsorption capacity (mg/g), C_0 is the initial surfactant concentration (mg/mL), C_e is the final surfactant concentration (mg/mL), m is the mass of the adsorbent (g), and V is the volume of the solution (mL).

After conducting the experiments, it was possible to construct adsorption isotherms, representing the curve of the solute quantity on the adsorbent (q) relative to the final concentration (C_e). Subsequently, to evaluate the adequacy of the models and adsorption mechanisms employed in this study, the experimental data were fitted to the Langmuir, Freundlich, and Sips isotherms, according to Equations (3), (4), and (5), respectively.

$$q_e = q_\infty \frac{K_L C_e}{1 + K_L C_e} \quad (3)$$

$$q_e = K_F C_e^{1/n} \quad (4)$$

$$q_e = q_\infty \frac{(K_S C_e)^{1/\beta}}{1 + (K_S C_e)^{1/\beta}} \quad (5)$$

where

- q_e is the adsorption capacity (mg of surfactant/g of rock);
- K_L is the Langmuir constant, the theoretical adsorption capacity on the monolayer ($L \cdot mg^{-1}$);
- C_e is the adsorbate concentration at equilibrium ($mg \cdot mL^{-1}$);
- K_F is the Freundlich constant ($L \cdot mg^{-1}$);
- $1/n$ is the empirical parameter that quantifies the heterogeneity of adsorption; the higher the value of n , the more heterogeneous the adsorption process;
- q_∞ is the maximum constant of adsorbate that can be adsorbed, i.e., it is the saturation value of q_e ($mg \cdot g^{-1}$);
- K_S is the Sips constant;
- β is the exponent of the Sips model.

The equilibrium time was determined through finite bath adsorption experiments at various time intervals (10 min, 30 min, 60 min, 200 min, 300 min, 360 min, and 1440 min) at a temperature of 298.15 K (25 °C). The selection of these parameters was based on previously published results [36,37,43,46,47]. All the samples had an initial surfactant concentration of 0.3%.

The experimental data, which shows the concentration of the adsorbed surfactant in the solid phase concerning the equilibrium concentration in the fluid phase, was analyzed using the Langmuir, Freundlich, and Sips models. The parameters and coefficients of determination (R^2) of the sorption isotherms were calculated through the least squares method for linear regression, utilizing OriginPro® 2021 software.

3. Results

3.1. Correlation between Surfactant Concentration and Surface Tension

Generally, ionic surfactants tend to present elevated CMC values due to the electrostatic interactions resulting from the ionic polarity of their molecules. It was observed that both SCO and SBCO exhibited CMC values of 0.0091 g/mL and 0.0011 g/mL, respectively. Coconut oil primarily consists of short-chain saturated fatty acids, characterized by single bonds, making them more prone to breakage (dodecanoic acid). Consequently, this structure has lower steric hindrance, promoting interaction between the liquid and solid phases.

On the other hand, SMO revealed an intermediate CMC value (0.0021 g/mL). This surfactant consists of unsaturated fatty acids, such as ricinoleic acid ((R,Z)-12-hydroxyoctadec-9-enoic acid), which is the primary component of castor oil and contains the OH functional

group on one of the carbon atoms. The molecular structures of the surfactants used in this study are shown in Figure 1.

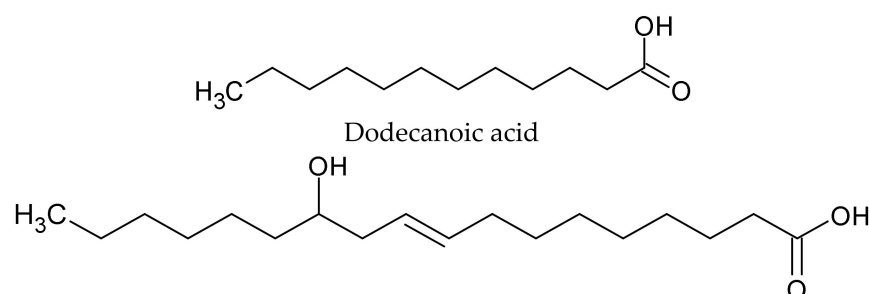


Figure 1. Molecular structures of surfactants based on coconut oil and castor oil, respectively.

This molecular arrangement helps enhance its solubility, resulting in the decrease in the CMC value. SCO has a higher CMC value due to two factors: its significant negative surface charge and the phenomenon of repulsion between the heads of the anionic surfactants when adsorbed at the liquid–gas interface. Research by Silva et al. [43] and colleagues showed that to achieve interface saturation and subsequent micelle formation, larger quantities of surfactant need to be added, indicating a higher surfactant concentration.

3.2. Experimental Design—Evaluation of Systems with Higher Adsorption Capacity

With the aim of optimizing the adsorption processes, an experimental design was employed to identify the optimal points for each adsorption assay. Initially, the surface tensions of the pure surfactant solutions were measured with a concentration of 0.3%. The results from the experimental design, along with the measurements of surface tensions of the filtrates for the three plant-based surfactants, are presented in Table 1. Overall, it was possible to observe an adsorption efficiency ranging from 19.34% to 85.74%, confirming that the variables R/S, t, and T directly affect the adsorption process.

Table 1. Experiment planning results for adsorption efficiency (AE%) of SCO, SBCO and SMO surfactants on carbonate rock.

Samples	SCO						SBCO			SMO		
	R/S (mL)	T (h)	T (°C)	ST (Dyn/cm)	C _e ×10 ⁻³ (%)	AE (%)	ST (Dyn/cm)	C _e ×10 ⁻³ (%)	AE (%)	ST (Dyn/cm)	C _e ×10 ⁻³ (%)	AE (%)
1	1/40	2	30	54.23	1.3	55.78	61.3	1.1	62.38	42.03	2.0	34.36
2	1/80	2	30	51.00	1.8	40.14	59.31	1.4	53.25	41.4	2.1	28.63
3	1/40	4	30	66.30	0.4	85.74	66.13	0.6	77.80	43.4	1.6	45.30
4	1/80	4	30	48.26	2.3	22.60	60.46	1.2	58.77	41.79	2.0	32.24
5	1/40	2	60	65.21	0.5	84.20	61.72	1.1	64.07	42.04	2.0	34.45
6	1/80	2	60	47.86	2.4	19.65	55.93	2.0	32.40	41.05	2.2	25.23
7	1/40	4	60	63.77	0.5	81.92	63.22	0.9	69.50	41.53	2.1	29.85
8	1/80	4	60	47.99	2.4	20.62	54.96	2.2	24.84	40.48	2.4	19.34
9	1/60	3	45	48.39	2.3	23.54	68.32	0.5	82.52	43.18	1.7	43.67
10	1/60	3	45	48.39	2.3	23.54	68.25	0.5	82.38	42.91	1.7	41.61
11	1/60	3	45	48.36	2.3	23.33	68.25	0.5	82.35	42.78	1.8	40.60

The ability of an oil to adsorb onto carbonates is related to its affinity with the carbonate rock surface and the properties of the oil components. In general, the adsorption capacity is influenced by the oil polarity and the presence of active compounds that can interact with the rock surface. Among babassu coconut oil, coconut oil, and castor oil, the surfactants in coconut oils showed the highest adsorption efficiencies on carbonates due to their lower polarity compared to the surfactants in saponified castor oil.

This is because coconut oil is mainly composed of saturated fatty acids, which tend to be less polar. Saturated fatty acids have a molecular structure that lacks double bonds between the carbon atoms, resulting in a linear carbon chain. This straight and non-double bond structure makes saturated fatty acids less polar compared to the unsaturated fatty

acids found in larger quantities in the other oils. Thus, the non-polar nature of this oil enables a robust interaction with carbonate surfaces, enhancing adsorption.

In the specific case of castor oil, it contains a high proportion of a specific fatty acid called ricinoleic acid, which is an unsaturated fatty acid that contains a hydroxyl on the twelfth carbon atom (from the carboxyl), which makes these oils more polar. As a result, castor oil may have weaker interactions with the non-polar surfaces of carbonate rocks. Additionally, the presence of double bonds in the unsaturated fatty acids makes castor oil less non-polar than coconut oils, leading to lower adsorption and a tendency to be solubilized in the aqueous medium. Throughout the adsorption process, molecules at the interface attract each other, causing a reduction in interfacial free energy.

On hydrophobic surfaces (weakly charged or not electrically charged), hydrophobic interaction is the main mechanism for the adsorption of surfactants in aqueous media, with the polar part facing the water. In particular, the adsorption of these surfactants on limestone is possibly due to the high solubility caused by their carboxylate groups. It is proposed that an interdigitated bilayer (surfactants alternating up and down) is formed on the carbonate rocks. This representation can be seen in Figure 2a,b.

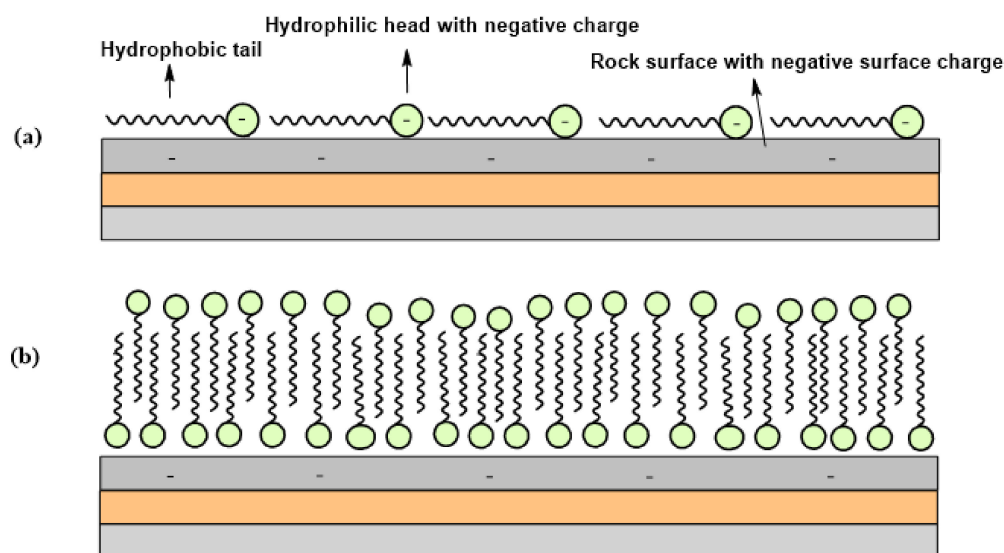


Figure 2. Adsorption mechanism proposed for anionic surfactants (SCO, SBCO, and SMO) on limestone, in which their polar tails face the surface of the rock (a), and a second layer is formed on top of the first, thus forming a bilayer (b).

Analysis of Figure 2 reveals that hydrophobic interaction played a key role in the adsorption of the anionic surfactants. The lipophilic nature (apolar tail) of the surfactants results in water repulsion, leading these molecules to come out of solution and migrate to the limestone surface (Figure 2a).

At this stage, the surfactants stabilize, with their lipophilic chains facing the surface of the rock and the hydrophilic chains facing the water, forming a layer of surfactants (Figure 2b). As the surfactant concentration increases, the molecules organize themselves into different shapes until they form a bilayer through hydrophobic interactions between the surfactant tails (Figure 2b).

The highest adsorption efficiency indices were achieved in assay 3 for SCO (reaching 85.74%), at the central point (9, 10, and 11) for SBCO (reaching 82.52%), and in assay 3 for SMO (reaching 45.30%). These were the systems chosen to more intrinsically evaluate the surfactant adsorption mechanisms in the rock. Based on the response surfaces in Supplementary Materials in Figures S1–S3, saponified plant surfactants are promising for treating reservoir rock surfaces and can therefore be applied to increase oil recovery in reservoir rocks. Their ability to reduce interfacial tensions between water and oil

through chemical interactions among fluids suggests significant potential for optimizing this process.

3.3. Characterization of Adsorbents

3.3.1. X-Ray Fluorescence and X-Ray Diffraction

The results of X-ray fluorescence analysis of the carbonate rock revealed a predominance of calcium oxide, CaO (93.95%), accompanied by small proportions of sodium oxide, Na₂O (1.5%), and magnesium oxide, MgO (1.4%). Additional impurities are present in reduced amounts and apparently did not play a significant role in the adsorption of anionic surfactants, as the main interaction occurs with Ca²⁺ and Mg²⁺ ions. XRF analysis also confirmed that the MgO content in limestone is less than 5%, characterizing it as calcitic limestone. These observations are fully aligned with the typical chemical compositions of these minerals.

The X-ray diffractograms agreed with the chemical composition determined by X-ray fluorescence, as illustrated in Figure 3. In the limestone sample, peaks correspond to calcite (CaCO₃). These diffraction patterns were compared with the ICDD/PDF 028827 database using PANalytical High Score software, according to the pattern marking, hydrated calcite has space group R-3c, with lattice parameters a, b, and c of 6.36; α, β, and γ of 46.1; and a unit cell volume of 121.85 Å³. The calcite reflections in limestone were determined by the peak of highest intensity (in 2θ 29°) reinforcing the characteristics of calcitic limestone. Figure 3 also shows that calcite (CaCO₃) constitutes the main mineral component of limestone, where adsorption of anionic surfactants occurs, resulting in a negative surface charge. Thus, X-ray fluorescence (XRF) and X-ray diffraction (XRD) analyses confirmed that the limestone used can be categorized as calcitic due to its low magnesium oxide content.

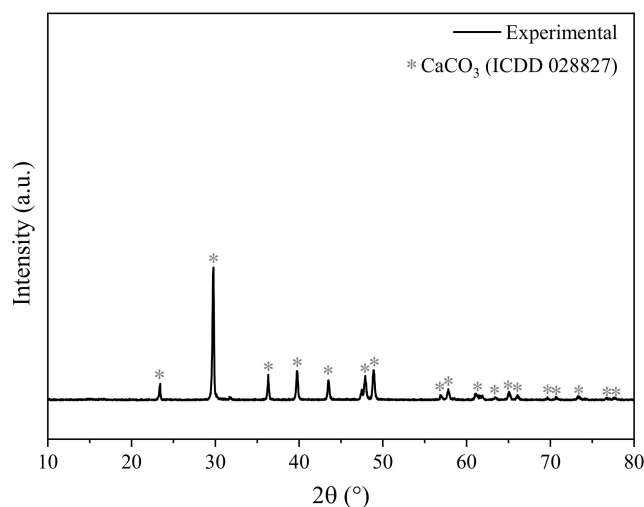


Figure 3. Limestone diffractogram.

3.3.2. Differential Thermal Analysis and Thermogravimetric Analysis (DTA/TGA)

The physico-chemical characterization of limestone rocks was carried out through immediate analysis and study of thermal behavior using thermogravimetric analysis (TGA/DTG), both before and after chemical treatment with the surfactants. The results are presented in Figure 4. In the curve of Figure 4A, an endothermic peak around 809.3 °C can be identified, accompanied by an approximate mass loss of 50%. It can be observed that these carbonates decompose at temperatures above 750 °C, according to the thermal decomposition reaction described below [32]:



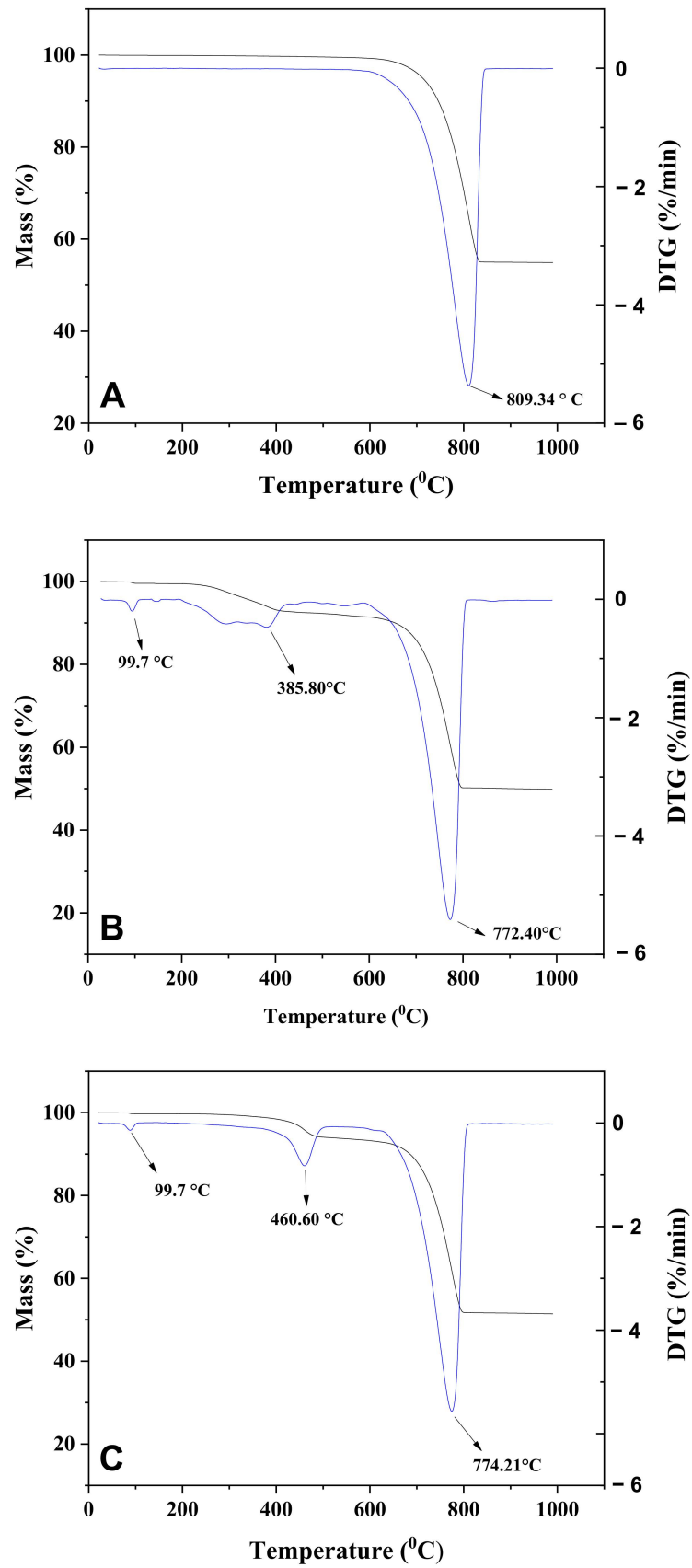


Figure 4. Cont.

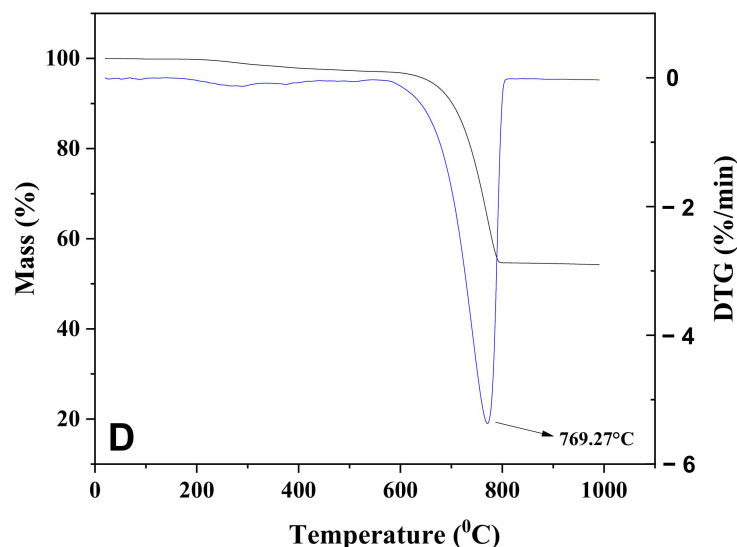


Figure 4. TG and DTG curves relative to (A) carbonate rock; (B) carbonate rock + SCO; (C) carbonate rock + SBCO and (D) carbonate rock + SMO.

Figure 4B corresponds to the limestone sample after the adsorption test with the SCO surfactant solution. The graph displays three distinct thermal events related to mass loss. The first occurs at temperatures near 100 °C, corresponding to water release. The second, between 230 °C and 400 °C, is associated with the boiling point and degradation of the surfactant. The third event, with temperatures above 760 °C, is attributed to the thermal decomposition of calcium carbonate, resulting in the formation of calcium oxide and the release of carbon dioxide. The mass losses correspond to 0.27%, 6.22%, and 39.23%, respectively.

The TGA curves in Figure 4B,C show similar behavior, as both surfactants originate from coconut, differing mainly in some chemical properties, such as boiling temperature. The mass losses correspond to 0.15%, 4.22%, and 37.91% for the samples of limestone + SBCO. Regarding Figure 4D, which involves limestone + SMO, it is observed that this surfactant exhibits few curves in its DTG, indicating its thermal stability against limestone thermal degradation. Castor oil contains about 90% ricinoleic acid, which gives it atypical characteristics, including a high boiling temperature around 313 °C, resulting in a limited thermo-oxidative degradation range for this surfactant. The mass loss for the limestone + SMO samples is approximately 34.52%.

3.3.3. Fourier Transform Infrared Spectroscopy (FTIR)

The infrared vibrational spectra corresponding to limestone are presented in Figure 5. The positions of the bands demonstrate coherence with the vibrations of carbonate ions present in calcite. The most prominent vibrational event in calcium carbonate materials is the asymmetric stretching of the carbonate ion, which appears in an approximate range of 1397–1420 cm^{-1} for calcite. Based on this information, it is possible to infer that the adsorbent is characterized as calcitic carbonate rock, showing characteristic carbonate bands at 1795 cm^{-1} , 1397–872 cm^{-1} , and 713 cm^{-1} , which correspond to the angular deformations of the CO_3^{2-} , C-O, and C=O bonds, respectively.

Analyzing the spectrum, the main bands referring to the presence of surfactants occur between 3000 and 2850 cm^{-1} and are attributed to the axial deformation vibrations of the C-H bonds of the methyl (CH_3) and methylene (CH_2) groups. These bands are characteristic of these components, thus indicating the presence of free fatty acids on the surface of the rock. These characteristics suggest adsorption of the surfactant in the rock structure. The bands show a decrease in intensity for the SMO adsorbed on the rock, indicating a variation in the interaction. The adsorption efficiency rates exceeded 80%, 82%, and 45% for SCO, SBCO, and SMO, respectively.

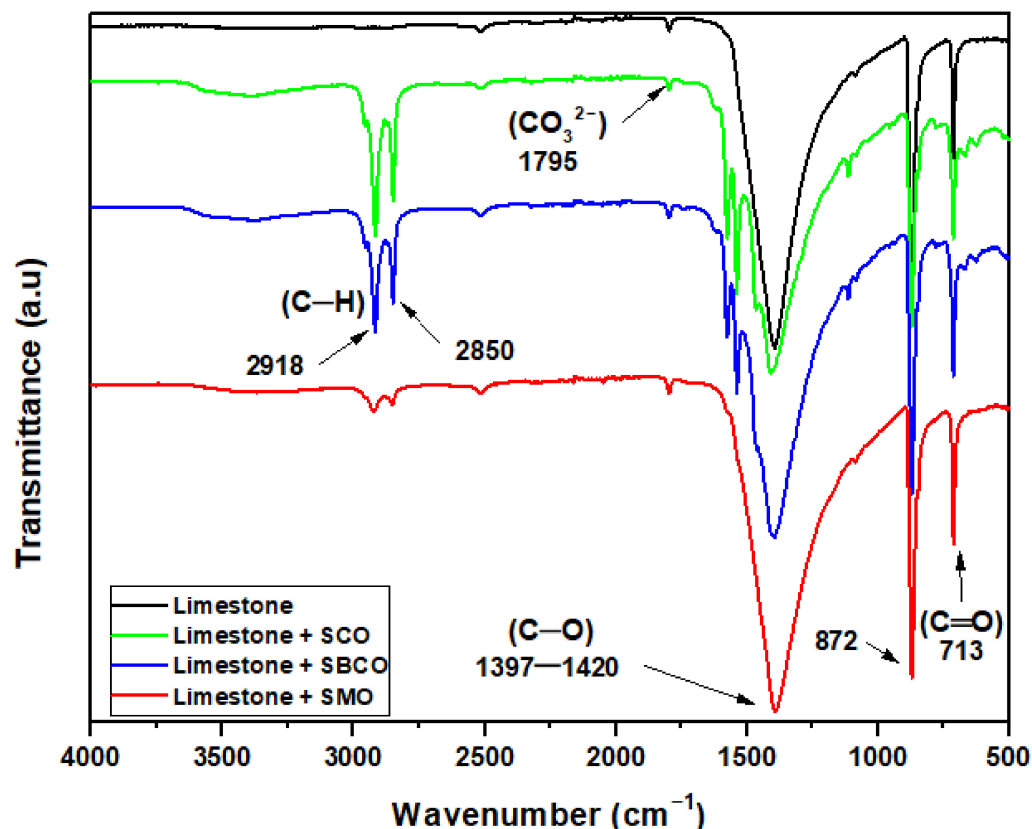


Figure 5. Infrared spectra of untreated and surfactant-treated carbonate rock samples.

3.3.4. Zeta Potential

The standard average zeta potential values for the water + limestone samples are -34.9 mV at pH 6.50. It is observed that the limestone used has a negative surface charge, with an approximate potential of -35.0 mV, indicating that calcitic limestone possesses an excess of negatively charged ions in solution. These electronegative particles remain in suspension, increasing the ion proportion in the solution. To investigate the electric charges on the solid surface when in contact with the adsorbates, zeta potential measurements were conducted, varying the pH of the surfactant solutions at a concentration of 0.3%. These measurements were performed after the finite bath assay for 2 h in contact with limestone, as illustrated in Figure 6.

The biodegradable surfactants were shown to have an isoelectric point below pH 7. In acidic conditions, all assays resulted in a zeta potential equal to zero, with most occurring around pH 4.33. The quantity of surfactants adsorbed on limestone surfaces is influenced by both the nature of the adsorbent surface and environmental conditions, including factors such as pH, temperature, and surfactant concentration in the system.

The efficiency of adsorption of these surfactants on limestone is due to its hydrophilic surface and electrostatic interactions between the adsorbent and the adsorbate. As the medium becomes alkaline (pH > 7), an increase in the potential in modulus is observed, reaching 84.8 mV at pH approximately equal to 12.00. This response was expected, considering the saponaceous nature of the surfactant and hence the high concentrations of OH^- ions.

Wang et al. [26] investigated the adsorption of an ionic surfactant on limestone and found that the greater the negative zeta potential, the higher the adsorption. The molecular structure of the biodegradable surfactants is similar, as they represent long-chain carboxylic acids (fatty acids). Together with limestone, the system gives a basic pH and high negative potential values, consistent with the literature.

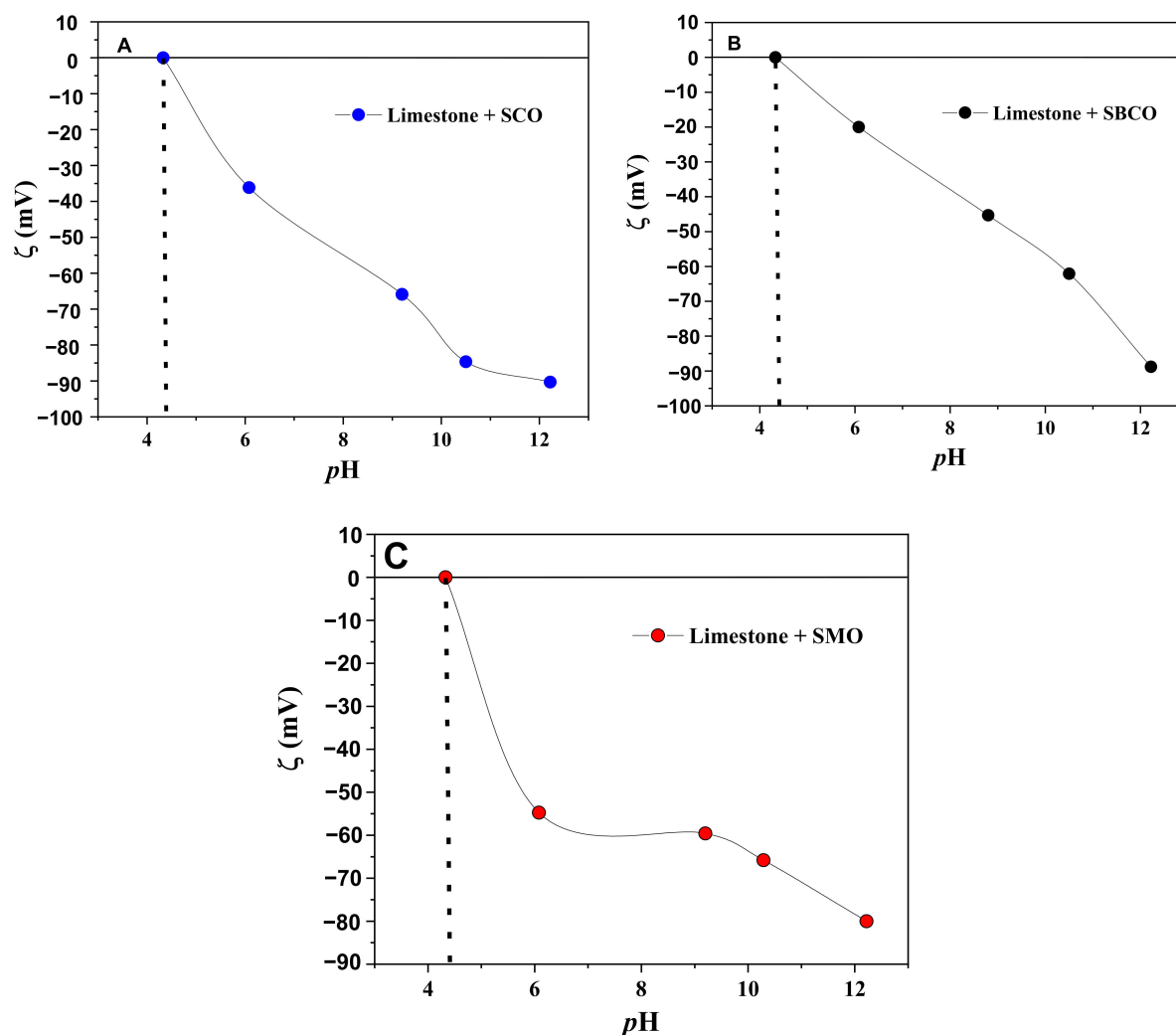


Figure 6. Zeta potential for 0.3% solutions of (A) SCO, (B) SBCO, and (C) SMO in limestone.

3.3.5. Scanning Electron Microscopy (SEM)

Scanning electron microscopy was used to investigate the morphology of the rock surface as well as its composition, aiming to evaluate the adsorption of anionic surfactants on the limestone surface. Figure 7 presents the results of SEM analysis of the rock surfaces before and after the static adsorption experiments. It was observed that calcitic limestone exhibits a compact structure, along with pores and an uneven surface with steps (Figure 7A). The calcination step resulted in a reduction in the average particle diameter, evident in the fragments displayed in the micrographs. This may have contributed to enhanced adsorption, resulting in an increase in the surface area.

Analysis of these micrographs shows that the interfacial spaces, i.e., the pores in the adsorbed limestone, were maintained after the adsorption tests with the surfactants. This is discernible from the morphological aspect, which reveals the distribution of the surfactants in the porous medium. Figure 7 illustrates the porosity present, as well as the thin layer of surfactants on the surface. This analysis only allows observation of the enlarged area on the surface of the particles and cannot cover the entire surface of the particles present in the samples. However, sites with particles of approximately similar size and shape were selected to investigate their morphology. Finally, calcination reduced the average particle diameter, increasing its surface area and the contact area with the surfactants. This fact emphasizes the importance of particle size regarding the kinetics of calcination and adsorption.

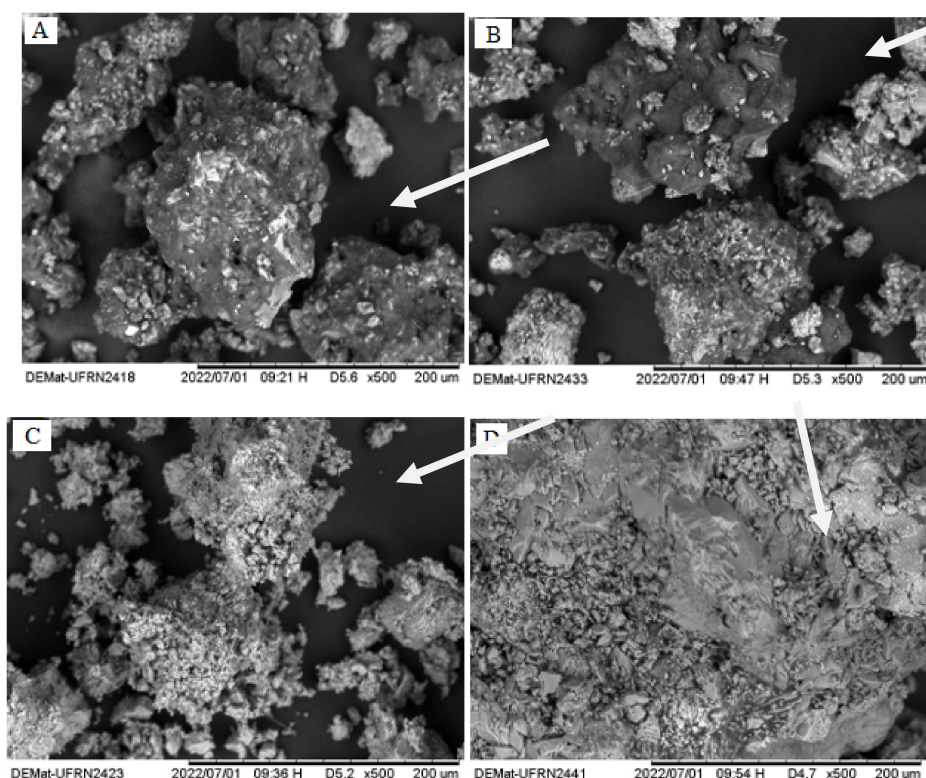


Figure 7. Micrographs of limestone (A) pre-adsorption; (B–D) after adsorption of the surfactants SCO, SBCO, and SMO, respectively, with a magnification of 500 \times . The arrows show the treated rock surfaces.

3.4. Adsorption Isotherms

To evaluate the adsorption capacity of anionic surfactants on limestone, finite batch tests were conducted to obtain isotherms and determine which adsorption models best fit these isotherms. Throughout the adsorption process, there is an attraction between molecules at the interface, resulting in a decrease in interfacial free energy. On hydrophobic surfaces (slightly charged or non-electrically charged), hydrophobic interaction is the main mechanism of surfactant adsorption in aqueous media, with the polar part facing the water.

Remarkably, there was higher adsorption of SCO, SBCO, and SMO on limestone compared to sandstone, possibly due to the high solubility of these surfactants, caused by their carboxylate groups. It is proposed that an interdigitated bilayer (surfactants alternating with heads up and down) is formed on the carbonate rocks. Indeed, an additional factor contributing to the lipophilic repulsion mechanism was the interaction between the negative surface charge of carbonate (zeta potential of -34.9 mV) and the negative carboxylate ions ($R-COO^-$) of the anionic surfactants.

For a better understanding of the adsorption mechanisms and to quantify the data, Langmuir, Freundlich, and Sips models were applied to fit the experimental results, which can be verified in the Supplementary Materials in Tables S2–S4. SCO fitted both the Langmuir model (indicating monolayer adsorption) and the Sips model. This behavior is evidenced in the q_e versus C_e graph for the experimental data in Figure 8.

Both SBCO and SMO fit well only to the Sips model, with R^2 values of 0.9692 and 0.9133, respectively. This adsorption isotherm considers the heterogeneity of the adsorbent surface, meaning it considers that the surface of the adsorbent material may have different adsorption sites with distinct affinities. Additionally, the model also accounts for interactions between the adsorbed molecules [23].

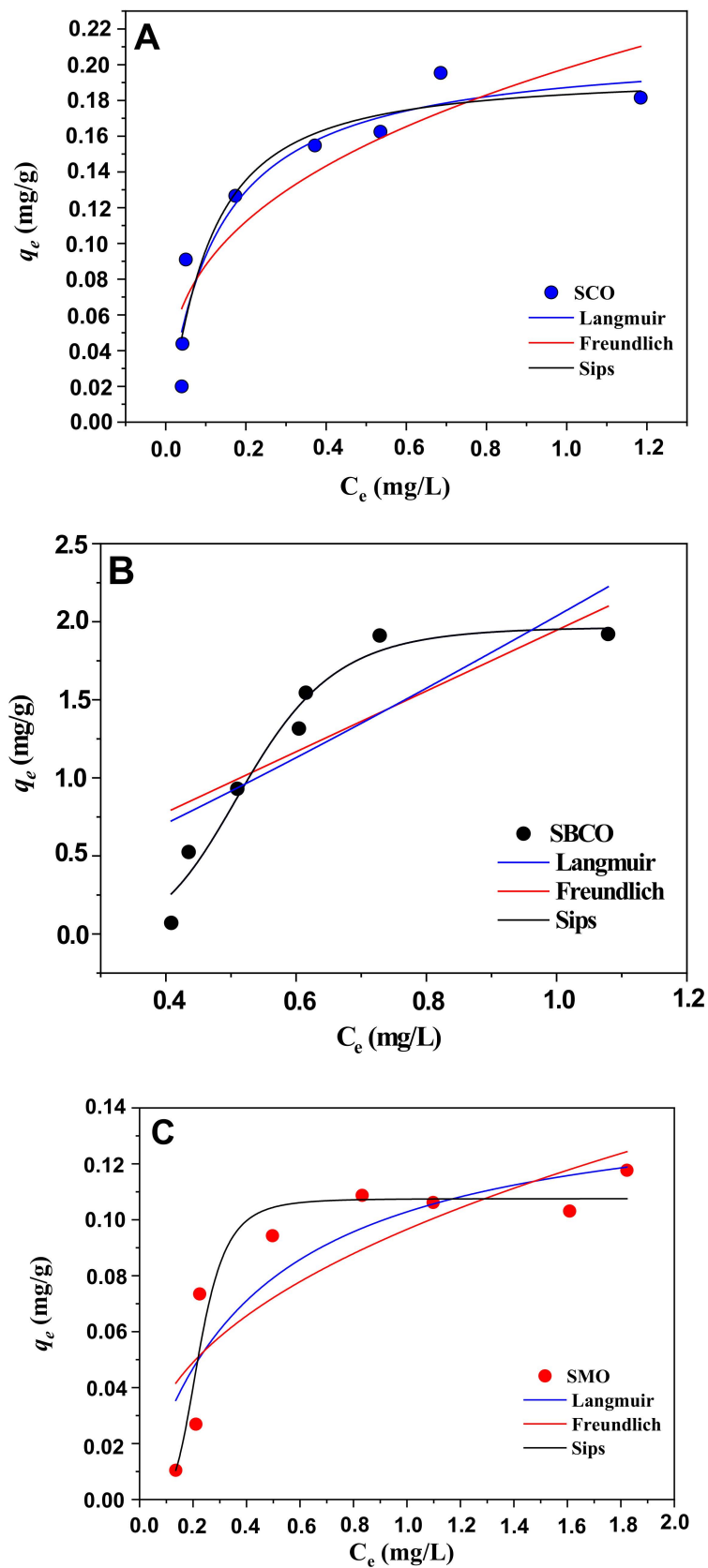


Figure 8. Graph of the adsorption isotherm of (A) OCS (pH = 10.5), (B) OCBS (pH = 10.3), and (C) OMS (pH = 10.1), and the curves obtained by fitting the Langmuir, Freundlich, and Sips models ($T = 303$ K).

At low adsorbate concentrations, the equation simplifies to the Freundlich isotherm, while at high concentrations, the model predicts a monolayer adsorption capacity, characteristic of the Langmuir isotherm. Moreover, it is observed that for the Freundlich model, the correlation coefficients are low, indicating that this model does not adequately describe the system.

Considering the parameters presented, it is observed that they fit better with the Sips model, especially at a temperature of 303 K. On the other hand, the parameters obtained from the Freundlich model confirm that this is the isotherm that least fits the experimental data. In addition to the low correlation, the error obtained was the highest within this study.

Influence of Temperature on SCO Adsorption Isotherms on Limestone

Figure 9 displays the adsorption isotherms of SCO on limestone at 298 K, 313 K, and 333 K. As the concentration of SCO increases, a rapid increase in adsorption is initially observed. This increase is progressively less effective as the curves reach the plateau. It is noted that adsorption is more pronounced at 333 K and more moderate at 298 K, indicating that adsorption is favored at higher temperatures. For a better understanding of the adsorption mechanism and to quantify the adsorption data, Langmuir and Freundlich models were applied to fit the experimental data at three different temperatures.

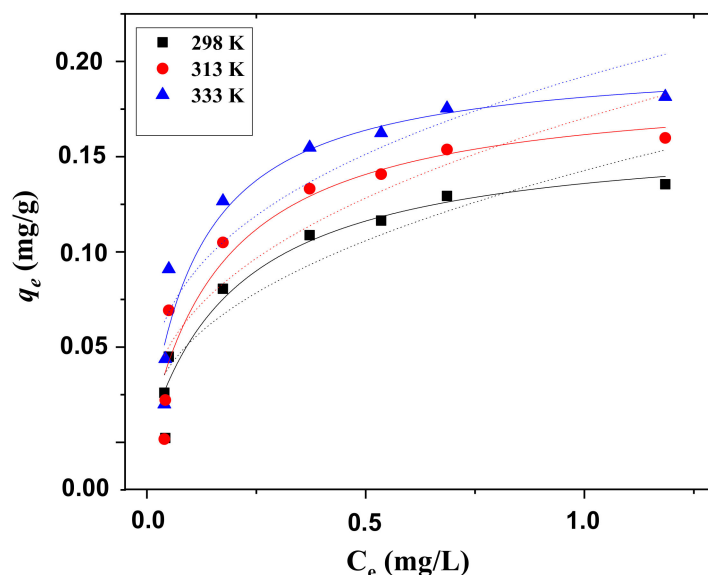


Figure 9. Adsorption isotherms of SCO on limestone at three different temperatures (298 K, 313 K, and 333 K), at pH = 10.5. The solid points represent the experimental data. The solid lines represent the Langmuir model. The dashed lines represent the Freundlich model.

Upon examining the SCO adsorption isotherms, it was found that the Langmuir model demonstrated greater efficacy in simulating these data compared to the Freundlich model, at temperatures of 298 K, 313 K, and 333 K. These results suggest that SCO adsorption predominantly occurs through a monolayer coverage mechanism on the adsorbent particles. The consistency of the experimental data with the Langmuir isotherm strengthens this conclusion, indicating that OCS adsorption is characterized by a single layer of adsorbed molecules on the surface of the adsorbent material. The corresponding parameters for both models are detailed in Table 2. The values of q_∞ calculated using the Langmuir model were lower at 298 K and higher at 333 K, which indicates that the adsorption of SCO on limestone is enhanced with increasing temperature.

Table 2. Parameters for the Langmuir and Freundlich isotherm models at different temperatures.

Langmuir Model				Freundlich Model		
T (K)	q_{∞} (mg/L)	K_L (L mg ⁻¹)	R ²	K_F (L mg ⁻¹)	1/n	R ²
298	4.884	0.164	0.914	2.991	0.345	0.842
313	5.743	0.203	0.922	2.246	0.408	0.830
333	8.432	0.190	0.950	2.011	0.431	0.880

4. Conclusions

The adsorption of three types of anionic surfactants onto limestone grain particles in aqueous solution was carefully studied. The adsorption efficiency, kinetics, and thermodynamics were obtained through experimental investigations. X-ray fluorescence (XRF) and X-ray diffraction (XRD) analyses show that the limestone used in this research can be classified as calcitic due to its low magnesium oxide content. The physicochemical characterization of the adsorbents, before and after treatment with anionic surfactants, revealed significant adsorption on the limestone surface.

The hydrophobic interaction between the tail of the surfactants and the negative surface of the limestone emerged as the main adsorption mechanism. This phenomenon was considered the driving force of limestone-surfactant adsorption. Infrared spectroscopy analysis revealed the adsorption of surfactants, suggesting the formation of covalent bonds between the surfactant and the limestone through chemical interactions. The adsorption efficiency rates exceeded 80%, 82%, and 45% for SCO, SBCO, and SMO, respectively. Temperature played a significant role in the maximum adsorption of SCO, being more effective at higher temperatures (30 °C, 45 °C, and 60 °C).

The pseudo-second-order kinetic model provided the best fit to the experimental data of the three investigated surfactants. Regarding the isotherms, the Sips model described the adsorption processes and mechanisms with greater accuracy, with determination coefficients (R²) of 0.92, 0.97, and 0.91 for SCO, SBCO, and SMO, respectively, at 30 °C.

Saponified plant surfactants look promising for the treatment of rock surfaces with a view to their application in enhanced oil recovery from waste rock, as they suggest an effective method for optimizing this process due to their ability to reduce interfacial tensions between water and oil through chemical interactions between fluids. The results of this study have significant implications for understanding the interactions between surfactants and rocks, as well as for future applications of these compounds in optimizing enhanced oil recovery. This work opens the door for more effective and sustainable approaches in developing techniques that maximize the treatment of reservoir rocks.

Supplementary Materials: The following supporting information can be downloaded at: <https://www.mdpi.com/article/10.3390/coatings14070856/s1>, Figure S1. Response surfaces for adsorption efficiency (% AE) of the surfactant OCS (a) t vs. R/S (b) T vs. R/S and (c) T vs. t, where R/S is the mass ratio of rock (g) per volume of surfactant solution in contact (mL), T is the temperature set in the system, and t is the contact time of the surfactant solution with the rock. The variable values are encoded as (−1, 0, and +1); Figure S2. Response surfaces for adsorption efficiency (% AE) of the surfactant OCBS (a) t vs. R/S (b) T vs. R/S and (c) T vs. t, where R/S is the mass ratio of rock (g) per volume of surfactant solution in contact (mL), T is the temperature set in the system, and t is the contact time of the surfactant solution with the rock. The variable values are encoded as (−1, 0, and +1); Figure S3. Response surfaces for adsorption efficiency (% AE) of the surfactant OMS (a) t vs. R/S (b) T vs. R/S and (c) T vs. t, where R/S is the mass ratio of rock (g) per volume of surfactant solution in contact (mL), T is the temperature set in the system, and t is the contact time of the surfactant solution with the rock. The variable values are encoded as (−1, 0, and +1). Table S1: Levels assumed for the influencing parameters in the adsorption tests; Table S2: Langmuir, Freundlich, and Sips isotherm parameters for OCS adsorption on limestone at 303 K. Table S3: Langmuir, Freundlich, and Sips isotherm parameters for the adsorption of OCBS on limestone at 303 K; Table S4: Langmuir, Freundlich, and Sips isotherm parameters for OMS adsorption on limestone at 303 K.

Author Contributions: Conceptualization, formal analysis, writing—review and editing, writing—original draft preparation V.F.d.S.B.; methodology, investigation, resources V.F.d.S.B. and D.C.d.S.; software, D.C.d.S.; validation, E.D.d.S.F., A.O.W.N. and T.P.B.; data curation, E.D.d.S.F. and D.C.d.S.; visualization, M.K.S.M. and J.L.C.F.; supervision, project administration A.O.W.N. All authors have read and agreed to the published version of the manuscript.

Funding: This research received no external funding.

Institutional Review Board Statement: Not applicable.

Informed Consent Statement: Not applicable.

Data Availability Statement: The data presented in this study are available upon request from the corresponding author.

Acknowledgments: The authors would like to thank the Surfactant Technology and Separation Processes Laboratory (LTT/IQ/UFRN) and laboratory of Membranes and Colloids (LAMECO/IQ/UFRN) of the Federal University of Rio Grande do Norte (UFRN) for offering the space, equipment and techniques used in this manuscript; and special thanks to Coordenação de Aperfeiçoamento de pessoal de Nível Superior (CAPES), Laboratório de Eletroquímica Ambiental e Aplicada (LEAA) and Pró-Reitoria de Pesquisa da Universidade Federal do Rio Grande do Norte (PROPESQ-UFRN) for financial support during the course of this work.

Conflicts of Interest: The authors declare no conflicts of interest.

References

1. Sheng, J.J. Status of surfactant EOR technology. *Petroleum* **2015**, *1*, 97–105. [[CrossRef](#)]
2. Zhang, R.; Somasundaran, P. Advances in adsorption of surfactants and their mixtures at solid/solution interfaces. *Adv. Colloid Interface Sci.* **2006**, *123–126*, 213–229. [[CrossRef](#)]
3. Zhang, R.; Somasundaran, P. Aggregate formation of binary nonionic surfactant mixtures on hydrophilic surfaces. *Langmuir* **2005**, *21*, 4868–4873. [[CrossRef](#)] [[PubMed](#)]
4. Coutinho de Araújo, J.D.; de Oliveira, G.V.B.; Lourenço, M.C.d.M.; da Silva, D.C.; de Castro Dantas, T.N.; Rodrigues, M.A.F.; Wanderley Neto, A.d.O. Adsorption study of non-ionic ethoxylated nonylphenol surfactant for sandstone reservoirs: Batch and continuous flow systems. *J. Mol. Liq.* **2022**, *366*, 120313. [[CrossRef](#)]
5. Gogoi, S.B. Adsorption-Desorption of Surfactant for Enhanced Oil Recovery. *Transp. Porous Media* **2011**, *90*, 589–604. [[CrossRef](#)]
6. Druetta, P.; Picchioni, F. Surfactant flooding: The influence of the physical properties on the recovery efficiency. *Petroleum* **2020**, *6*, 149–162. [[CrossRef](#)]
7. Chen, Z.Z.; Gang, H.Z.; Liu, J.F.; Mu, B.Z.; Yang, S.Z. A thermal-stable and salt-tolerant biobased zwitterionic surfactant with ultralow interfacial tension between crude oil and formation brine. *J. Pet. Sci. Eng.* **2019**, *181*, 106181. [[CrossRef](#)]
8. Massarweh, O.; Abushaikha, A.S. The use of surfactants in enhanced oil recovery: A review of recent advances. *Energy Rep.* **2020**, *6*, 3150–3178. [[CrossRef](#)]
9. Negin, C.; Ali, S.; Xie, Q. Most common surfactants employed in chemical enhanced oil recovery. *Petroleum* **2017**, *3*, 197–211. [[CrossRef](#)]
10. De Araújo, C.R.B.; Da Silva, D.C.; Arruda, G.M.; Rodrigues, M.A.F.; Wanderley Neto, A.D.O. Removal of oil from sandstone rocks by solid-liquid extraction using oil phase-free microemulsion systems. *J. Environ. Chem. Eng.* **2021**, *9*, 104868. [[CrossRef](#)]
11. Chen, Y.; Ubaidah, A.; Elakneswaran, Y.; Niasar, V.J.; Xie, Q. Detecting pH and Ca²⁺ increase during low salinity waterflooding in carbonate reservoirs: Implications for wettability alteration process. *J. Mol. Liq.* **2020**, *317*, 114003. [[CrossRef](#)]
12. Alghamdi, A.O.; Abu-Al-Saud, M.O.; Al-Otaibi, M.B.; Ayirala, S.C.; Alyousef, A. Electro-kinetic induced wettability alteration in carbonates: Tailored water chemistry and alkali effects. *Colloids Surf. A Physicochem. Eng. Asp.* **2019**, *583*, 123887. [[CrossRef](#)]
13. Nowrouzi, I.; Mohammadi, A.H.; Khaksar Manshad, A. Double-Chain Single-Head modification of extracted saponin from *Anabasis Setifera* plant and its effects on chemical enhanced oil recovery process by surfactant-alkali slug injection into carbonate oil reservoirs. *J. Pet. Sci. Eng.* **2021**, *201*, 108438. [[CrossRef](#)]
14. Ahmadi, M.A.; Shadzadeh, S.R. Implementation of a high-performance surfactant for enhanced oil recovery from carbonate reservoirs. *J. Pet. Sci. Eng.* **2013**, *110*, 66–73. [[CrossRef](#)]
15. Saxena, N.; Goswami, A.; Dhodapkar, P.K.; Nihalani, M.C.; Mandal, A. Bio-based surfactant for enhanced oil recovery: Interfacial properties, emulsification and rock-fluid interactions. *J. Pet. Sci. Eng.* **2019**, *176*, 299–311. [[CrossRef](#)]
16. Lu, J.; Liyanage, P.J.; Solairaj, S.; Adkins, S.; Arachchilage, G.P.; Kim, D.H.; Britton, C.; Weerasooriya, U.; Pope, G.A. New surfactant developments for chemical enhanced oil recovery. *J. Pet. Sci. Eng.* **2014**, *120*, 94–101. [[CrossRef](#)]
17. Das, S.; Katiyar, A.; Rohilla, N.; Nguyen, Q.; Bonnecaze, R.T. Universal scaling of adsorption of nonionic surfactants on carbonates using cloud point temperatures. *J. Colloid Interface Sci.* **2020**, *577*, 431–440. [[CrossRef](#)] [[PubMed](#)]

18. Belhaj, A.F.; Elraies, K.A.; Mahmood, S.M.; Zulkifli, N.N.; Akbari, S.; Hussien, O.S.E. The effect of surfactant concentration, salinity, temperature, and pH on surfactant adsorption for chemical enhanced oil recovery: A review. *J. Pet. Explor. Prod. Technol.* **2020**, *10*, 125–137. [[CrossRef](#)]
19. Bera, A.; Kumar, T.; Ojha, K.; Mandal, A. Adsorption of surfactants on sand surface in enhanced oil recovery: Isotherms, kinetics and thermodynamic studies. *Appl. Surf. Sci.* **2013**, *284*, 87–99. [[CrossRef](#)]
20. Mao, J.; Wang, D.; Yang, X.; Zhang, Z.; Yang, B.; Zhang, C. Adsorption of surfactant on stratum rocks: Exploration of low adsorption surfactants for reservoir stimulation. *J. Taiwan Inst. Chem. Eng.* **2019**, *95*, 424–431. [[CrossRef](#)]
21. Li, X.; Zhang, J.; Tang, X.; Mao, G.; Wang, P. Study on wellbore temperature of riserless mud recovery system by CFD approach and numerical calculation. *Petroleum* **2020**, *6*, 163–169. [[CrossRef](#)]
22. Saha, R.; Uppaluri, R.V.S.; Tiwari, P. Effect of mineralogy on the adsorption characteristics of surfactant—Reservoir rock system. *Colloids Surf. A Physicochem. Eng. Asp.* **2017**, *531*, 121–132. [[CrossRef](#)]
23. Kalam, S.; Abu-Khamsin, S.A.; Kamal, M.S.; Hussain, S.M.S.; Norrman, K.; Mahmoud, M.; Patil, S. Adsorption Mechanisms of a Novel Cationic Gemini Surfactant onto Different Rocks. *Energy Fuels* **2022**, *36*, 5737–5748. [[CrossRef](#)]
24. Kalam, S.; Abu-Khamsin, S.A.; Kamal, M.S.; Patil, S. Surfactant Adsorption Isotherms: A Review. *ACS Omega* **2021**, *6*, 32342–32348. [[CrossRef](#)] [[PubMed](#)]
25. ShamsiJazeyi, H.; Hirasaki, G.J.; Verduzco, R. Sacrificial agent for reducing adsorption of anionic surfactants. *Proc. SPE Int. Symp. Oilf. Chem.* **2013**, *1*, 214–229. [[CrossRef](#)]
26. Wang, J.; Han, M.; Fuseni, A.B.; Cao, D. Surfactant adsorption in Surfactant-Polymer flooding for carbonate reservoirs. *SPE Middle East Oil Gas Show Conf. MEOS Proc.* **2015**, *2015*, 1736–1746. [[CrossRef](#)]
27. Lu, J.; Goudarzi, A.; Chen, P.; Kim, D.H.; Delshad, M.; Mohanty, K.K.; Sepehrnoori, K.; Weerasooriya, U.P.; Pope, G.A. Enhanced oil recovery from high-temperature, high-salinity naturally fractured carbonate reservoirs by surfactant flood. *J. Pet. Sci. Eng.* **2014**, *124*, 122–131. [[CrossRef](#)]
28. Ma, K.; Cui, L.; Dong, Y.; Wang, T.; Da, C.; Hirasaki, G.J.; Biswal, S.L. Adsorption of cationic and anionic surfactants on natural and synthetic carbonate materials. *J. Colloid Interface Sci.* **2013**, *408*, 164–172. [[CrossRef](#)] [[PubMed](#)]
29. Somasundaran, P.; Zhang, L. Adsorption of surfactants on minerals for wettability control in improved oil recovery processes. *J. Pet. Sci. Eng.* **2006**, *52*, 198–212. [[CrossRef](#)]
30. Somasundaran, P.; Hanna, H.S. Adsorption of Sulfonates on Reservoir Rocks. *J. Polym. Sci. Part A-2 Polym. Phys.* **1979**, *19*, 221–232. [[CrossRef](#)]
31. Jarrahian, K.; Seiedi, O.; Sheykhani, M.; Sefti, M.V.; Ayatollahi, S. Wettability alteration of carbonate rocks by surfactants: A mechanistic study. *Colloids Surf. A Physicochem. Eng. Asp.* **2012**, *410*, 1–10. [[CrossRef](#)]
32. Neves, A.M.; Santanna, V.C.; Barillas, J.L.M.; Castro Dantas, T.N.; Góis, A.G.B. Ionic surfactants applied in enhanced oil recovery: Adsorption, imbibition, and zeta potential approaches. *Braz. J. Chem. Eng.* **2020**, *37*, 263–269. [[CrossRef](#)]
33. Paternina, C.A.; Londoño, A.K.; Rondon, M.; Mercado, R.; Botett, J. Influence of salinity and hardness on the static adsorption of an extended surfactant for an oil recovery purpose. *J. Pet. Sci. Eng.* **2020**, *195*, 107592. [[CrossRef](#)]
34. Da Silva, D.C.; dos Santos Lucas, C.R.; de Moraes Juviniiano, H.B.; de Alencar Moura, M.C.P.; Dantas Neto, A.A.; de Castro Dantas, T.N. Novel produced water treatment using microemulsion systems to remove oil contents. *J. Water Process Eng.* **2020**, *33*, 101006. [[CrossRef](#)]
35. Fuguet, E.; Ràfols, C.; Rosés, M.; Bosch, E. Critical micelle concentration of surfactants in aqueous buffered and unbuffered systems. *Anal. Chim. Acta* **2005**, *548*, 95–100. [[CrossRef](#)]
36. Prosser, A.J.; Franses, E.I. Adsorption and surface tension of ionic surfactants at the air-water interface: Review and evaluation of equilibrium models. *Colloids Surf. A Physicochem. Eng. Asp.* **2001**, *178*, 1–40. [[CrossRef](#)]
37. Warr, G.G. Surfactant adsorbed layer structure at solid/solution interfaces: Impact and implications of AFM imaging studies. *Curr. Opin. Colloid Interface Sci.* **2000**, *5*, 88–94. [[CrossRef](#)]
38. Shahrabadi, A.; Daghbandan, A.; Arabiyoun, M. Experimental investigation of the adsorption process of the surfactant-nanoparticle combination onto the carbonate reservoir rock surface in the enhanced oil recovery (EOR) process. *Chem. Thermodyn. Therm. Anal.* **2022**, *6*, 100036. [[CrossRef](#)]
39. Ahmadi, M.A.; Shadizadeh, S.R. Experimental investigation of adsorption of a new nonionic surfactant on carbonate minerals. *Fuel* **2013**, *104*, 462–467. [[CrossRef](#)]
40. Kalam, S.; Abu-Khamsin, S.A.; Gbadamosi, A.O.; Patil, S.; Kamal, M.S.; Hussain, S.M.S.; Al-Shehri, D.; Al-Shalabi, E.W.; Mohanty, K.K. Static and dynamic adsorption of a gemini surfactant on a carbonate rock in the presence of low salinity water. *Sci. Rep.* **2023**, *13*, 11936. [[CrossRef](#)]
41. Curbelo, F.D.S.; Santanna, V.C.; Neto, E.L.B.; Dutra, T.V.; Dantas, T.N.C.; Neto, A.A.D.; Garnica, A.I.C. Adsorption of nonionic surfactants in sandstones. *Colloids Surf. A Physicochem. Eng. Asp.* **2007**, *293*, 1–4. [[CrossRef](#)]
42. Anderson, W.G. Wettability Literature Survey—Part 1: Rock-Oil-Brine Interactions and the Effects of Core Handling on Wettability. *J. Pet. Technol.* **1986**, *38*, 1125–1144. [[CrossRef](#)]
43. Da Silva, D.C.; de Oliveira Wanderley Neto, A.; Peres, A.E.C.; Neto, A.A.D.; Dantas, T.N.C. Removal of oil from produced water by ionic flocculation using saponified babassu coconut oil. *J. Mater. Res. Technol.* **2020**, *9*, 4476–4484. [[CrossRef](#)]
44. Leyes, M.F.; Reyes, S.G.; Cuenca, E.; Morales, J.F.S.; Ritacco, H. Adsorption kinetics of a cationic surfactant bearing a two-charged head at the air-water interface. *Coatings* **2020**, *10*, 95. [[CrossRef](#)]

45. Guzmán, E.; Fernández-Peña, L.; Akanno, A.; Llamas, S.; Ortega, F.G.; Rubio, R. Two different scenarios for the equilibration of polycation—Anionic solutions at water–vapor interfaces. *Coatings* **2019**, *9*, 438. [[CrossRef](#)]
46. Filho, E.D.S.; Brito, E.L.; Nogueira, D.O.; Fonseca, J.L.C. Thermal degradation and drug sorption in hybrid interpolyelectrolyte particles. *Colloids Surf. A Physicochem. Eng. Asp.* **2021**, *610*, 125894. [[CrossRef](#)]
47. French, R.O.; Wadsworth, M.E.; Cook, M.A.; Cutler, I.B. The quantitative application of infrared spectroscopy to studies in surface chemistry. *J. Phys. Chem.* **1954**, *58*, 805–811. [[CrossRef](#)]

Disclaimer/Publisher’s Note: The statements, opinions and data contained in all publications are solely those of the individual author(s) and contributor(s) and not of MDPI and/or the editor(s). MDPI and/or the editor(s) disclaim responsibility for any injury to people or property resulting from any ideas, methods, instructions or products referred to in the content.